Synthesis and Structural Study on MnO_2 Nanosheet Material by X-ray Absorption Spectroscopic Technique

Yoshihiro Kadoma,[†] Yoshiharu Uchimoto,[‡] and Masataka Wakihara*,[†]

Department of Applied Chemistry, Tokyo Institute of Technology, Ookayama, Meguro-ku, Tokyo 152-8552, Japan, and Department of Interdisciplinary Environment, Graduate School of Human and Environmental Studies, Kyoto University, Yoshida-nihonmatsu-cho, Sakyo-ku, Kyoto 606-8501, Japan

Received: July 13, 2005; In Final Form: September 2, 2005

MnO_2 nanosheet with acetylene black composite material has been synthesized from layered $K_{0.45}MnO_2$ powder. The electrochemical lithiation reaction of nanosheet composite material proceeds in a different manner from that of the parent material, layered $K_{0.45}MnO_2$ powder. To elucidate the origin of the changes in discharge profile, the electronic and local structures for the nanosheet composites and its parent and protonated material have been investigated by Mn *K*-edge and O *K*-edge X-ray absorption spectroscopy (XAS). The results showed that local and electronic structure around Mn ions does not vary during nanosheet formation, while significant changes in electronic structure around oxide ions were observed. Accordingly, it is suggested that the difference observed in discharge profile is due to the electronic structural change induced by nanosheet formation.

Introduction

It is important to investigate the electrochemical reaction mechanism at the electrode/electrolyte interface, not only for the fundamental electrochemistry but also for the development of electrochemical applications, such as lithium ion battery, fuel cell, etc. Most of the interfacial electrochemical reaction studies have been performed by single crystals of noble metals (such as Pt and Au). On the other hand, 3d transition metal oxides are especially attractive for the practical use of electrochemical devices;[1−6] therefore, the knowledge about detailed interface reaction mechanism between electrode/electrolyte is strongly demanded. Nevertheless, few papers in this field have been reported, mainly due to the difficulty of characterizing the surface structure of transition metal oxides. Recently, Sasaki et al.[7] reported the preparation of MnO_2 nanosheets that have many characteristic features as a single crystal in two dimensions: molecular size thickness, micro size width of face, large surface area, and so forth (see Figure 1).[8−10] Therefore, the plane surface being perpendicular to the *z*-axis dominantly forms an interface with electrolyte solutions, giving us the concrete image regarding the electrochemical reaction with MnO_2 nanosheet. Hence, a detailed investigation of the nanosheet surface structure is required.

This paper describes the synthesis procedure of the MnO_2 nanosheet and changes in the electronic and local structures for the nanosheet, which were investigated by using Mn *K*-edge and O *K*-edge XAS.[11−12] Electrochemical lithiation reaction was also studied to reveal the difference in equilibrium state between the nanosheet and bulk MnO_2 structure.

Experimental Section

Sample Preparation. Layered-type $K_{0.45}MnO_2$ (see Figure 1) was synthesized by conventional solid-state reaction as described in ref 8. A stoichiometric mixture of K_2CO_3 (Wako Pure Chemical Industries) and Mn_2O_3 was heated at 800 °C for 30 h under an O_2 gas flow. [Mn_2O_3 was prepared by the calcination of $MnCO_3$ (99.9%, Soekawa Chemicals) at 600 °C for 48 h in air.]

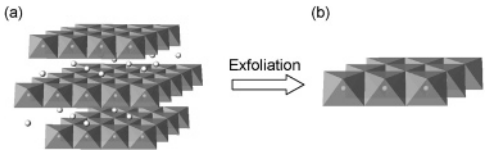

Figure 1. Schematic figure of the exfoliation: (a) layered $K_{0.45}MnO_2$ powder and (b) MnO_2 nanosheet.

Protonated layered $K_{0.45}MnO_2$ was prepared by soaking 5 g of $K_{0.45}MnO_2$ in 1 dm^3 of a 1 mol dm^{-3} HCl aqueous solution under stirring for 10 days. HCl solution was refreshed every day to promote complete protonation. The resulting material was washed and air-dried at ambient temperature, yielding the protonated material. Then, the colloidal suspension of MnO_2 nanosheet was prepared by vigorously stirring 0.2 g of the protonated material in 500 cm^3 of tetra-*n*-butylammonium hydroxide [$(C_4H_9)_4NOH$] solution at room temperature for 10 days. Acetylene black (AB) was mixed with the colloidal suspension (the ratio of AB and colloidal suspension was 9:1, w/w) and thereafter was vigorously agitated at room temperature for 6 h. The water was evaporated by agitating the solution at 80 °C. After the composite suspension was evaporated for 1 week, the composite material was obtained by vacuum-drying at 100 °C for 1 day. The protonation and exfoliation process was followed according to the previous report.[8]

Characterization. Crystalline phase identification was carried out by powder X-ray diffraction (XRD) on a Rigaku RINT2500V diffractometer, with Cu Kα radiation (λ = 0.154 05 nm), equipped with a curved graphite monochromator, at room temperature.

XAS experiments were performed at the synchrotron facility, Photon Factory (PF; Tsukuba, Japan). Mn *K*-edge and O *K*-edge X-ray absorption near-edge structure (XANES) and extended

* Corresponding author: tel +81-3-5734-2145; fax +81-3-5734-2146; e-mail mwakihar@o.cc.titech.ac.jp.
[†] Tokyo Institute of Technology.
[‡] Kyoto University.

10.1021/jp053854k CCC: $33.50
Published on Web 12/13/2005

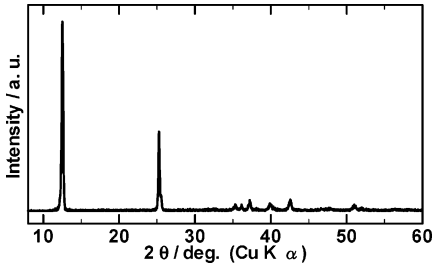

Figure 2. XRD pattern for the layered $K_{0.45}MnO_2$ powder as synthesized.

X-ray absorption fine structure (EXAFS) spectra were measured in order to clarify the change in electronic structure and local symmetry. O *K*-edge XANES spectra were measured at BL 11A beam lines at PF by the method of total electron yields at room temperature. Mn *K*-edge EXAFS measurements were performed at BL 9A and 12C beam lines at PF, at room temperature in transmission mode with gas ionization detectors. The appropriate amount of each sample powder for EXAFS measurement (determined to obtain suitable X-ray absorption) was mixed with 200 mg of boron nitride as a binder. The absolute energy scales were calibrated by using the value of Mn metal. Fourier transformations were performed over the *k* range 3−12 $Å^{-1}$ with k^3 weighting. The structural parameters were determined by curve-fitting procedures with Rigaku REX2000 data analysis software.[13] Theoretical parameters of backscattering factors and phase shifts used in the curve-fitting analysis were calculated by FEFF8 (multiple-scattering XAS simulation code: see details in refs 14 and15).

Electrochemical Lithiation. The electrochemical lithiation was performed with a three-electrode-type cell. The ratio of the composite electrode for this measurement of the parent material was 70 wt % active materials of sample, 25 wt % acetylene black, and 5 wt % poly(tetrafluoroethylene) (PTFE), while the electrode of the nanosheet composite was composed of 90 wt % active materials and 10 wt % PTFE. Lithium foil was used as counterelectrode and reference electrode, with current collectors of aluminum mesh. The electrolyte used was 1 mol dm^{-3} $LiClO_4$ in 1:1 (v/v) ethylene carbonate (EC)/diethyl carbonate (DEC) solution (Tomiyama Pure Chemical Industries Ltd). All of the experiments were carried out galvanostatically at 10 μA cm^{-2} in an Ar-filled glovebox at room temperature. The cutoff potentials were set at 2.0 V (vs Li/Li^+) and 4.3 V.

Results and Discussion

The powder XRD pattern for the layered $K_{0.45}MnO_2$ powder is showed in Figure 2, in good agreement with the previously reported data.[16] Two intense diffraction peaks at 12.5° and 25.1° can be indexed as 001 and 002 in the hexagonal cell. Accordingly, remarkable preferred orientation is observed.

The discharge profile of the layered $K_{0.45}MnO_2$ powder is represented in Figure 3a. During the first discharge curve, the layered $K_{0.45}MnO_2$ powder indicates a pseudoplateau near 3.1 V due to the redox reaction of the Mn^{3+}/Mn^{4+} couple.[17] Figure 3b shows the charge−discharge profiles of the nanosheet composite material of MnO_2 nanosheet mixed with acetylene black. In the case of the nanosheet composite, the initial charge capacity indicates the removal of tetra-*n*-butylammonium hydroxide cations, which were used for exfoliation of layered $K_{0.45}MnO_2$. On the other hand, the first discharging of the nanosheet composite illustrated continual decrease in its voltage diagrams from 4.0 to 2.0 V with capacity of ca. 150 mA h g^{-1}, which is comparable to that of layered $K_{0.45}MnO_2$. Such a

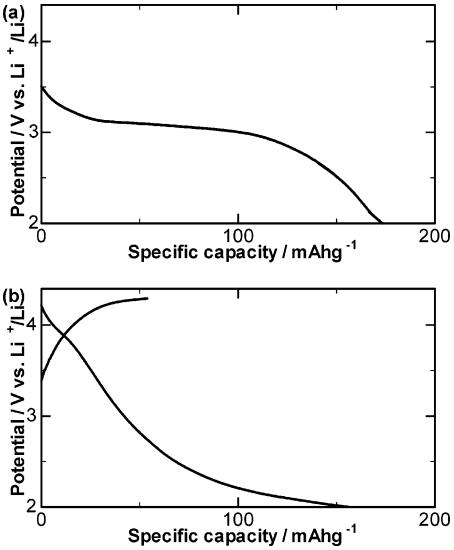

Figure 3. Charge−discharge profiles of (a) layered $K_{0.45}MnO_2$ powder and (b) nanosheet composite material. Current density was 10 μA cm^{-2}; cutoff potential was 2.0−4.3 V.

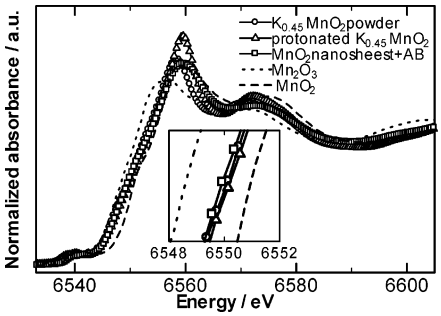

Figure 4. Mn *K*-edge XANES spectra of layered $K_{0.45}MnO_2$ powder (○) protonated material (△), and nanosheet composite material (□), with Mn_2O_3 (···) and MnO_2 (− − −) for reference.

difference in discharge profile of layered $K_{0.45}MnO_2$ and the nanosheet composite would result from the difference between the lithium ion insertion into bulk structure of MnO_2 and adsorption onto surface structure. Since the cell potential in the discharge process was affected by the crystal and electronic structure of host materials, the following section will describe them by means of the XAS technique.

It is well-known that the X-ray absorption near-edge structure (XANES) technique is sensitive to the electronic configuration and local environment around X-ray absorbed atoms, such as valence state, chemical bonding character, local coordination, and so on. To clarify the changes in electronic structure and local symmetry for the prepared sample, Mn *K*-edge and O *K*-edge XANES spectra were measured. Figure 4 depicts the Mn *K*-edge XANES spectra for the nanosheet composite material, its parent material, and protonated material, together with the data for reference compounds Mn_2O_3 and MnO_2, where the valence states of manganese ions are +3 and +4, respectively. The absorption edge energy of the nanosheet composite does not change from the parent and protonated materials, indicating that the valence states of manganese ions in three samples are almost the same.[18] Chances are the cations of ammonium hydroxide are replaced by H^+ on the nanosheet surface to maintain charge neutrality during the exfoliation process. Considering the XANES spectra of the reference materials, the valence states of manganese ions for the prepared samples are between +3 and +4, which is in good agreement with previous reports and also the expectation from the formula

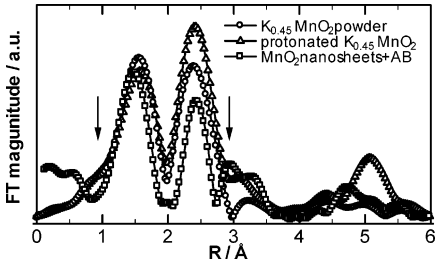

Figure 5. Fourier transforms of Mn *K*-edge EXAFS spectra of layered $K_{0.45}MnO_2$ powder (○), protonated material (△), and nanosheet composite material (□). The range over which Fourier filtering has been applied is shown by the arrows.

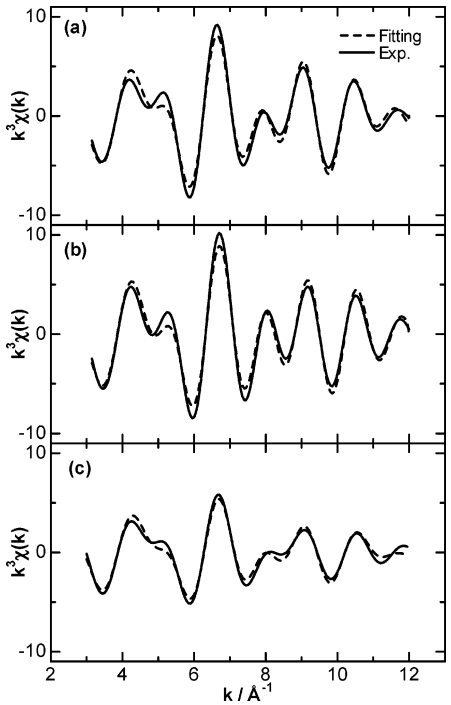

Figure 6. Inverse Fourier transforms of Mn *K*-edge EXAFS spectra of (a) layered $K_{0.45}MnO_2$ powder, (b) protonated material, and (c) nanosheet composite material.

of $K_{0.45}MnO_2$ (the formal oxidation state of manganese ions should be +3.55). In addition, it is noted that the difference in the shape of the spectra for the protonation and exfoliation of layered $K_{0.45}MnO_2$ shows no considerable change. Therefore, the local environment with respect to the crystal and electronic structure was kept unchanged during the reaction mentioned above.

The local structure of manganese ion in the layered $K_{0.45}MnO_2$ powder, protonated material, and nanosheet composite material was investigated by the EXAFS technique. As shown in Figure 5, the k^3-weighted Mn *K*-edge EXAFS spectra for the samples are Fourier-transformed (FT) in the *k* range 3.0−12.00 $Å^{-1}$. All of the FT spectra, which show pseudoradial distribution functions, exhibit two intense peaks at 1.5 and 2.5 Å attributed to the Mn−O and Mn−Mn interactions, respectively. To perform the nonlinear curve-fitting analysis, the FT spectra are inversely Fourier-transformed to *k* space as shown in Figure 6, and the two-shell model composed of Mn−O and Mn−Mn with six coordinates was adopted for the fittings (the range over which Fourier filtering has been applied is shown by the arrows in Figure 5). The results of fitted structural parameters are summarized in Table 1. The validity of the present fitting results was supported by relatively small residues

TABLE 1: Mn *K*-Edge EXAFS Spectra Determined Structural Parameters[a] for Layered $K_{0.45}MnO_2$ Powder, Protonated Material, and Nanosheet Composite Material

	Mn−O			Mn−Mn			residue[c]
	CN[b]	*R*/Å	*σ*/Å	CN[b]	*R*/Å	*σ*/Å	(%)
layered $K_{0.45}MnO_2$ powder	6	1.899	0.053	6	2.894	0.043	2.943
protonated $K_{0.45}MnO_2$	6	1.893	0.063	6	2.864	0.036	3.746
MnO_2 nanosheet + AB	6	1.904	0.075	6	2.888	0.087	3.348

[a] CN, coordination number; R, bond length; *σ*, Debye−Waller factor. [b] Fixed parameter for the curve-fitting procedure. [c] Residue = $100\sum\{k^3\chi_{obs}(k) - k^3\chi_{calc}(k)\}^2/\sum\{k^3\chi_{obs}(k)\}^2$.

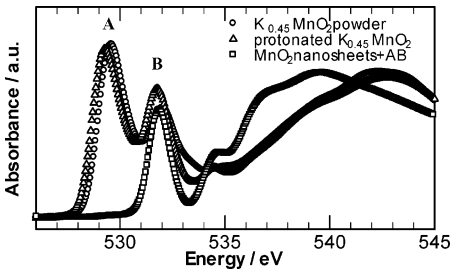

Figure 7. O *K*-edge XANES spectra of layered $K_{0.45}MnO_2$ powder (○), protonated material (△), and nanosheet composite material (□).

($R < 4.0$ %) and good accord between observed and simulated EXAFS oscillation shown in Figure 6. As seen in Table 1, no marked changes in interatomic distances were observed with protonation and exfoliation reaction (the changes are less than ~1.0 %), indicating the oxidation state and local coordination environment around manganese ions are unchanged between bulk and nanosheet materials.

Figure 7 shows the O *K*-edge XANES spectra for the nanosheet composite material and the parent and protonated materials. It is known that the broad peaks at more than about 535 eV correspond to the transition from O 1s to the mixing bands of O 2p and Mn 4sp orbital, while the features around 530 eV are ascribed to the transition from O 1s to the mixing bands of O 2p and Mn 3d orbital.[19−20] The peak feature in the O *K*-edge XANES for the layered $K_{0.45}MnO_2$ powder is almost the same as the protonated material, implying that the electronic structure of two samples is unchanged by protonation. Two intensive absorption peaks at 529 eV (peak A in Figure 7) and 532 eV (peak B in Figure 7) were observed in the parent and protonated materials. On the other hand, the peak at 529 eV (peak A) disappears in the nanosheet composites, and large spectral difference was also observed in O 2p−Mn 4sp hybridized level. Therefore, it is revealed that the exfoliation reaction caused electronic structural changes around oxide ions but roughly no changes around manganese ions. The formation of dangling bonds on the nanosheet surface, which is due to the breakage of the oxygen bond during exfoliation, would cause significant changes in O *K*-edge XANES, meaning electronic structural changes around oxide ions.

Summing up, the difference in electronic structure between nanosheet and bulky MnO_2 is observed only around oxide ions, while no marked change was observed around manganese ions. Therefore, the electrochemical behaviors of lithiation into layered material and adsorption onto nanosheet would strongly depend on the difference in electronic structure because there is no considerable change around manganese ions.

Acknowledgment. The present work was supported in part through a Grant-in-Aid for Scientific Research on Priority Area, Nanoionics (439) by the Ministry of Education, Culture, Sports, and Technology and Science. Y. K. thanks the 21st-century COE

program—Creation of Molecular Diversity and Development of Functionalities (B07)—by the Ministry of Education, Culture, Sports, Technology and Science (MEXT), Japan. XAS measurement has been performed under the approval of the Photon Factory Program Advisory Committee (Proposals 2002G254, 2003G260, and 2003G262).

References and Notes

(1) Dahn, J. R.; Von Sacken, U.; Juzkow, M. W.; Al-Janaby, H. *J. Electrochem. Soc.* **1991**, *138*, 2207.

(2) Scrosati, B. *Nature* **1995**, *373*, 557.

(3) Armstrong, A. R.; Bruce, P. G. *Nature* **1996**, *381*, 499.

(4) Tarascon, J.-M.; Armand, M. *Nature* **2001**, *431*, 170.

(5) Shao, Z.; Haile, S. M. *Nature* **2004**, *414*, 359.

(6) Adcock, P. A.; Pacheco, S. V.; Norman, K. M.; Uribe, F. A. *J. Electrochem. Soc.* **2005**, *152*, A459.

(7) Sasaki, T.; Watanabe, M.; Hashizume, H.; Yamada, H.; Nakazawa, H. *J. Am. Chem. Soc.* **1996**, *118*, 8329.

(8) Wang, L. Z.; Omomo, Y.; Sakai, N.; Fukuda, K.; Nakai, I.; Ebina, Y.; Takada, K.; Watanabe, M.; Sasaki, T. *Chem. Mater.* **2003**, *15*, 2873.

(9) Nakato, T.; Miyamoto, N.; Harada, A.; Ushiki, H. *Langmuir* **2003**, *19*, 3157.

(10) Sakai, N.; Ebina, Y.; Takada, K.; Sasaki, T. *J. Am. Chem. Soc.* **2004**, *126*, 5851.

(11) Stōhr, J. *NEXAFS Spectroscopy*; Springer-Verlag: Berlin, 1992.

(12) Koningsberger, D. C.; Prins, R. *X-ray Absorption: Principles, Applications, Techniques of EXAFS, SEXAFS and XANES*; Wiley: New York, 1988.

(13) Rigaku EXAFS Analysis Software, REX2000, Rigaku Co., 2003.

(14) Ankudinov, A. L.; Ravel, B.; Rehr, J. J.; Conradson, S. D. *Phys. Rev. B* **1998**, *58*, 7565.

(15) Ankudinov, A. L.; Bouldin, C.; Rehr, J. J.; Conradson, S. D. *Phys. Rev. B* **2002**, *65*, 104102.

(16) Delmas, C.; Fouassier, C. *Z. Anorg. Allg. Chem.* **1976**, *420*, 184.

(17) Ohzuku, T.; Kitagowa, M.; Hiral, T. *J. Electrochem. Soc.* **1990**, *17*, 769.

(18) Wang, L.; Takada, K.; Kajiyama, A.; Onoda, M.; Michiue, Y.; Zhang, L.; Watanabe, M.; Sasaki, T. *Chem. Mater.* **2003**, *15*, 4508.

(19) Groot, F. M. F.; Grioni, M.; Fuggle, J. C.; Ghijsen, J.; Sawatzky, G. A.; Petersen, H. *Phys. Rev. B* **1989**, *40*, 5715.

(20) Abbate, M.; Groot, F. M. F.; Fuggle, J. C.; Fujimori, A.; Strebel, O.; Lopez, F.; Domke, M.; Kaindl, G.; Sawatzky, G. A.; Takano, M.; Takeda, Y.; Eisaki, H.; Uchida, S. *Phys. Rev. B* **1992**, *46*, 4511.